Charge Puddles and the Edge Effect in a Graphene Device as Studied by a Scanning Gate Microscope

J. Chae[1], S. Y. Jung[2,3], S. J. Woo[4], H. J. Yang[1+], H. Baek[1], J. Ha[1], Y. J. Song[2,3], Y.-W. Son[4], N. B. Zhitenev[2], J. A. Stroscio[2], and Y. Kuk[1,*]

[1]Department of Physics and Astronomy, Seoul National University, Seoul 151-747, Korea, [2]Center for Nanoscale Science and Technology, National Institute of Science and Technology, Gaithersburg, MD 20988, USA, [3]Maryland NanoCenter, University of Maryland, College Park, MD 20742, USA, [4]School of Computational Sciences, Korea Institute for Advanced Study, Seoul 130-722, Korea

Despite the recent progress in understanding the geometric structures of defects and edges in a graphene device (GD), how such defects and edges affect the transport properties of the device have not been clearly defined. In this study, the surface geometric structure of a GD was observed with an atomic force microscope (AFM) and the spatial variation of the transport current by the gating tip was measured with scanning gate microscopy (SGM). It was found that geometric corrugations, defects and edges directly influence the transport current. This observation is linked directly with a proposed scattering model based on macroscopic transport measurements.

*To whom correspondence should be addressed to: ykuk@phya.snu.ac.kr

+Present address: Samsung Advanced Institute and Technology, Gyeonggi-do, 449-712, Korea

INTRODUCTION

Graphene has been widely studied due to scientific interests and because of its possible application to high-speed devices [1-4]. Ever since the successful separation of graphene layers, many unique physical properties of graphene have been reported, including its linear dispersion relationship, relativistic fermionic behavior in the conduction and the valence bands, two-dimensional electron gas (2DEG) behavior, and back-scatteringless tunneling [5-9]. Many related theoretical predictions have been confirmed by macroscopic transport measurements [2,3,10]. Despite the successful explanation of the physical properties, the correlation between the geometric structures of defects such as those caused by corrugations, defects and edges and the carrier scattering at these defects is not fully understood. For example, the mobility of graphene measured in a suspended GD or epitaxially grown graphene is reportedly as high as 200,000 cm/V·s [11-16]. However, a GD on a SiO_2 substrate has been measured in the range of 5,000~10,000 cm/V·s [17-19]. The difference is modeled by the carrier scattering by various defects on a GD on SiO_2 substrate but not on a suspended GD. Thus far, structural studies have been conducted using microscopic tools such as electron microscopy and scanning tunneling microscopy [16,20-25], while the transport properties have been measured macroscopically in a two- or four-terminal device with a back gate [2].

We report local carrier transport measurement results using SGM. SGM is a unique microscopic tool with which the local geometric and electronic structures and the transport property of an electronic device can be measured simultaneously [26-34]. An SGM uses a conducting tip to apply an electric field locally and measures the transport current through two or four contacts. It can use the same tip to measure the geometric structure in Atomic Force Microscopy (AFM) mode. The results of this experiment showed that the local geometrical defects indeed work as scattering centers in the transport measurement.

TRANSPORT PROPERTY of GD

Even before any transport measurement of a GD were reported, Ando predicted the characteristics of the transport properties [35]; perfect graphene only with short-range scatters would show no conductivity dependence on the carrier density because the scattering rate would be divergent as the carrier density goes to zero near the Dirac point. However, the long-range scatters would be dominant in the low-density limit such that the device becomes

insulating at the Dirac point. Earlier transport results reported that the conductivity is linearly dependent on the induced charge density by the back gate voltage, even in the range of $\pm 1 \times 10^{13}$ cm^{-2} [2,3]. This result suggests that the transport property of a GD is strongly dependent on the scattering mechanism by long-range scatters. With the progress of GD fabrication, a GD was processed as a suspended device in order to remove the substrate effects [14,15]. It was predicted that the carrier transport would be affected by scattering with charged impurities, short-range scatterers, mid-gap states, various phonon modes, surface corrugations, and defects in a GD [17-19,36-40]. In the case of the charged impurity potential at a high carrier density limit, the conductance is given by

$$\sigma = C \frac{e^2}{h} \left| \frac{n}{n_{imp}} \right| \qquad (1)$$

which is linearly dependent on the induced charge density [17,38]. The dimensionless constant C is ~10 to ~20. A recent experiment reported that the measured mobility is linearly dependent on the doping level of potassium [38,41].

Experimentally, the existence of charge puddle in graphene on the top of the SiO$_2$ substrate was resolved using a scanning single-electron transistor microscope [42]. That experimental result was considered in the theoretical calculation of transport properties of GD near Dirac point [43]. Recently, another investigation resolved the charge impurity scattering centers using a spatial map in scanning tunneling spectroscopy (STS). In that study, the Dirac point was locally mapped from STS data and the scattering pattern was analyzed to determine the scattering centers. Good agreement was noted between the local Dirac point and a theoretical model of carrier scattering [44].

Another important scattering mechanism in a GD is scattering with a phonon. Raman spectroscopy results in the presence of an electric field showed G band damping due to scattering with a phonon [40]. The temperature-dependent resistivity of GD is well-fitted to the theoretical prediction considering the scattering with an acoustic and an optical phonon [18]. Scattering by geometric corrugations on a graphene surface is also an interesting subject. The corrugations can be formed by interaction with the substrate or by a thermal cycle during the annealing process [45]. From the theoretical calculations, electrons in the presence of a ripple are affected by the vector potential due to a strain field [37,46]. However, the role of corrugation in carrier transport remains not well understood.

SCANNING GATE MICROSCOPE

The SGM in this study was operated under an ultrahigh vacuum (UHV) at 20 K with liquid helium, at 84K with liquid nitrogen, and at room temperature. The sample can be annealed with current through a device or annealing of the whole chamber can be accomplished at an elevated temperature. An ultra-sharp AFM tip can be positioned over the GD using custom-made vacuum motors. During the SGM operation, the transport current is measured through the electrodes, as shown in Fig. 1A. As we place the conducting AFM over the area of interest in a GD, the transport current varies as we move the device. A typical total conductance value without the tip gate is ~ 100 μS whereas the variation in the conductance with the tip gate is ~ 1 μS.

A custom-made UHV AFM operating at cryogenic temperatures was used to perform the SGM experiment, as shown in Fig. 1B [47]. The AFM head has a rigid three-column structure inside the UHV chamber, and the chamber is immersed in a liquid-helium Dewar and cooled by the helium exchange gas (at nearly one atmospheric pressure) to ensure optimal thermal and vibrational stability. The radiation through the main probe chamber is effectively cut off by internal baffles and the objective lens of the CCD optics is installed for a long-range optical microscope just above the AFM head. To achieve the maximum numerical aperture, we mounted an objective lens with a diameter of 25 mm and a focal length of 60 mm on top of the head. We drilled a small hole (4 mm diameters) in the lens along its optical axis to allow for the unhindered piezomotor-driven motion of the optical fibers. The intermediate image of the tip and the sample formed near the top of the main chamber is refocused onto the CCD by a telescopic microscope lens. Fig. 1C shows a long-range optical microscope image on the sample surface and the cantilever.

Vibration isolation is achieved by anchoring the chamber on a granite table. Three air table legs support the granite table, at 500 kg, and the cut off frequency is below ~3Hz. A helium Dewar is attached to three additional air dampers to isolate the mechanical vibration from the Dewar. The system is installed in a sound-proof room that is separate from the control and measurement circuits. The noise level from mechanical parts is much less than 100dB. A laser light bounced off the back of a commercial cantilever is detected by a quadrant photo diode to detect the z movement of the probe. The head has four inertial piezomotors: a one-dimensional (1D) Z motor [48] (10 mm span) for a coarse approach to the sample, and three planar XY motors (2 mm x 2 mm span each) for fine horizontal positioning of the sample and to adjust the laser lens assembly and the photodiode. A pan-type linear

walker with six independent shear piezo feet is used for coarse movement of the sample to the tip. As a white light source (the cleaved end of the multi-mode fiber) illuminates the sample surface at the angle θ, we can estimate the distance between the tip and the sample to be ten times the distance between the cantilever and its shadow laid on the sample, achieving a safe and fast coarse approach down to a tip-sample distance of ~ 5 µm.

SAMPLE PREPARATION

The GDs used in this study were fabricated by fabrication processes similar to those reported earlier [4]. Graphene flakes were mechanically exfoliated from either highly oriented pyrolitic graphite (HOPG) or natural graphite. Graphite was tapped onto scotch tape and then peeled off several times until it appeared shiny. Subsequently, this graphene tape was transferred by finger onto the top of thermally grown 300-nm thick SiO_2 on a highly doped Si substrate that was used as back gate later. The thickness of the graphene flake was confirmed by micro-Raman spectroscopy. A single layer of graphene was confirmed via image contrast of an optical microscope. Source-drain metal (3 nm Cr / 30 nm Au) contacts were defined by conventional electron beam lithography and a lift-off process. Figure 2A shows an optical image of a fabricated GD with metallic contacts. These electrodes were used as markers to position the sample with the tip later, as shown in Fig. 1B. After the GD was mounted in a cryogenic AFM, a macroscopic transport measurement was done to check the device characteristics, including the position of the Dirac point, electron and the hole mobility, as shown in Fig. 2B. Red and green lines represent data of a different sweep direction to note the hysteresis of the device. As the GDs were fabricated in an ambient environment and transferred to the AFM chamber, the macroscopic transport properties changed in the UHV chamber, as expected [49]. Figures 2C and D demonstrate the transport current as a function of the back gate bias voltage before the GD was inserted into a vacuum (2C) and in the vacuum (2D). Under ambient pressure, the Dirac point of the GD exceeded +20 V, indicating a hole-doped device by water molecule adsorption on graphene. After the GD was annealed at 380 K for 6 hours, the Dirac point moved to ~0 V, suggesting that the adsorbates were desorbed under UHV. The mobility of the sample was also increased when this process was repeated.

RESULTS and DISCUSSION

5

The topography of a graphene layer was measured using a scanning tunneling microscope (STM). In monolayer graphene, a honeycomb-shaped STM topography is observed. In double-layer graphene, every other carbon atom appears bright, resulting in a hexagonal topography due to the Bernal stacking of the double layers. Figure 3A shows an STM image of an epitaxially grown graphene layer on a Si-terminated SiC surface [50], showing the honeycomb-shaped atomic details. Imaging of the atomic details of a GD on SiO_2 was not possible with STM without an x-y motor or by the optical microscope in this chamber. In the SGM chamber, where x-y-z motors were equipped, it was possible to obtain a resolution of ~ 1nm with a cantilever-based operation. Figure 3B shows a STS result on the graphene layer. It has a hump just below the Fermi level, as explained by phonon-mediated tunneling near the Dirac point [25].

After a GD was installed in a cryogenic AFM-SGM chamber, it was imaged in AFM mode. Figure 4A shows a contact mode AFM image of a GD, where a SiO_2-coated Si tip was used. The GD appears to have a lighter color in the middle. The corrugation on the SiO_2 surface is known to be ~1 nm with an average corrugation width of ~50-60 nm [51]. Similar corrugation was observed on the GD, and the characteristic features are very similar on the GD and a SiO_2 substrate. Figure 4B shows the AFM topography of a GD with a higher resolution. Again, the observed corrugation depth is very similar to that on a SiO_2 surface and the average separation among those corrugations is ~50-60 nm, as reported on a bare SiO_2 surface. This data suggests if there is a scattering mechanism due to corrugation, it can be modeled by this topography. Unlike earlier results [36], we could not find self-similarity in the length scale in our data.

After the corrugation was confirmed by AFM topography, SGM experiments were conducted. Figure 5A depicts a 800 x 800 nm^2 AFM topography of a GD and Figs. 5B-L show SGM micrographs from a tip bias voltage range of –2.5 to +2.5 in steps of 0.5 V. The Dirac point of this GD was –24 V, as set by the back gate bias. All of the SGM measurements were taken at Dirac point by back-gating. Corrugations on graphene surface are seen in topography image with lateral dimension of ~100 nm. The spatial variations of conductance change become more prominent as the absolute value of the tip gate bias increases in either negative or positive polarity. Negative (positive) polarity of electric field from the tip is related to the scattering dynamics of electron (hole) carriers. The small features in the SGM data are tens of nanometers, revealing good agreement with the AFM observation. There is

strong correlation between the SGM signal and the topographic corrugations; the peaks appear at the bottom of the valley in topography. The range of high conductance region with hole carrier is extended more than that with electron carrier at the same electric field strength. This difference is due to the structure of charge puddle. The correlation between topographic data and SGM data implies that the charge puddles exist at the bottom of each ripple. The difference features in electron and hole carriers indicates that electrons are more locally confined at the bottom of the ripple induced by the interaction with substrate and hole carrier screens around confined electrons.

Unlike scattering by a geometrical corrugation, scattering caused by crystalline defects are slightly different. Figure 6A shows the topographic image with defect and Figs. 6B-F show the tip bias dependence of the SGM micrographs near defects with tip gating bias of −2.0 V (B),−4.0 V (C) , 0 V (D), 2.0 V (E) and 4.0 V (F) respectively. The nature of this defect is not clear, but this area appears to be elastically deformed. The SGM signal indicates strong carrier scattering even at a high tip bias voltage compared to scattering by geometrical corrugations in which the averaging effect by tip bias conceal the spatial resolution with tip gating voltage of higher than ±3 V [52]. It is worth to note that the conductance change by tip gating is dramatically high compared to scattering by geometrical corrugations. Color-coded scale bar for SGM signal for defect is shown in Fig. 6G which is an order of magnitude higher than that for geometrical corrugation as shown in Fig. 5M. This result indicates that the defect can affect the transport properties in a dramatic way and has to be considered carefully.

When the SGM signal was measured at edges of a GD, a strong enhancement of the SGM signal was observed. Figure 7A and B show SGM results obtained by contact mode AFM with SiO$_2$-coated Si tip. The Dirac point of this sample was –20 V according to the back gate bias. As the tip gate bias was decreased to –2V, Fig. 7B, i.e., as the tip gate approaches the Dirac point, the edge transport signal increases by as much as 10 times that at the middle of the GD. That is due to charge accumulation at the edge of a GD by electrostatic force [53]. The edge state conducting channel can be opened and contributed to electron transport like in a lightning rod. More experiment about edge effect with gate-controlled GD showed that the conductance enhancement at the edge was not observed with back gate of Dirac point (in low carrier density limit), however, the conductance enhancement at edge were observed again in electron or hole charging regime. Theoretical calculation with SGM simulation confirmed this edge effect by the edge channel opening [52]. Based on this result, it becomes necessary

to re-interpret a considerable amount of existing macroscopic data.

In conclusion, the results of this study show that geometric ripples, defects and edges directly influence the transport current according to SGM. This observation is directly linked with the proposed scattering model based on macroscopic transport measurements, and the existing results must be re-examined.

REFERNCES

[1]   K.S. Novoselov, A.K. Geim, S.V. Morozov, D. Jiang, Y. Zhang, S.V. Dubonos, et al., Electric Field Effect in Atomically Thin Carbon Films, Science. 306 (2004) 666-669.

[2]   K.S. Novoselov, A.K. Geim, S.V. Morozov, D. Jiang, M.I. Katsnelson, I.V. Grigorieva, et al., Two-dimensional gas of massless Dirac fermions in graphene, Nature. 438 (2005) 197-200.

[3]   Y. Zhang, Y. Tan, H.L. Stormer, P. Kim, Experimental observation of the quantum Hall effect and Berry's phase in graphene, Nature. 438 (2005) 201-204.

[4]   K.S. Novoselov, D. Jiang, F. Schedin, T.J. Booth, V.V. Khotkevich, S.V. Morozov, et al., Two-dimensional atomic crystals, Proceedings of the National Academy of Sciences of the United States of America. 102 (2005) 10451-10453.

[5]   A.H. Castro Neto, F. Guinea, N.M.R. Peres, Drawing conclusions from graphene, Physics World. 19 (2006) 33-37.

[6]   V.P. Gusynin, S.G. Sharapov, Unconventional Integer Quantum Hall Effect in Graphene, Phys. Rev. Lett. 95 (2005) 146801.

[7]   N.M.R. Peres, F. Guinea, A.H. Castro Neto, Electronic properties of disordered two-dimensional carbon, Phys. Rev. B. 73 (2006) 125411.

[8]   M.I. Katsnelson, K.S. Novoselov, A.K. Geim, Chiral tunnelling and the Klein paradox in graphene, Nat Phys. 2 (2006) 620-625.

[9]   M. Katsnelson, K. Novoselov, Graphene: New bridge between condensed matter physics and quantum electrodynamics, Solid State Communications. 143 (2007) 3-13.

[10]   A.F. Young, P. Kim, Quantum interference and Klein tunnelling in graphene heterojunctions, Nat Phys. 5 (2009) 222-226.

[11]   K. Bolotin, K. Sikes, Z. Jiang, M. Klima, G. Fudenberg, J. Hone, et al., Ultrahigh electron mobility in suspended graphene, Solid State Communications. 146 (2008) 351-355.

[12]   X. Du, I. Skachko, A. Barker, E.Y. Andrei, Approaching ballistic transport in suspended graphene, Nat Nano. 3 (2008) 491-495.

[13]   M. Orlita, C. Faugeras, P. Plochocka, P. Neugebauer, G. Martinez, D.K. Maude, et al., Approaching the Dirac Point in High-Mobility Multilayer Epitaxial Graphene, Phys. Rev. Lett. 101 (2008) 267601.

[14]   K.I. Bolotin, F. Ghahari, M.D. Shulman, H.L. Stormer, P. Kim, Observation of the fractional quantum Hall effect in graphene, Nature. 462 (2009) 196-199.

[15]   X. Du, I. Skachko, F. Duerr, A. Luican, E.Y. Andrei, Fractional quantum Hall effect and insulating phase of Dirac electrons in graphene, Nature. 462 (2009) 192-195.

[16]   D.L. Miller, K.D. Kubista, G.M. Rutter, M. Ruan, W.A. de Heer, P.N. First, et al., Observing the Quantization of Zero Mass Carriers in Graphene, Science. 324 (2009) 924-927.

[17]   Y. Tan, Y. Zhang, K. Bolotin, Y. Zhao, S. Adam, E.H. Hwang, et al., Measurement of Scattering Rate and Minimum Conductivity in Graphene, Phys. Rev. Lett. 99 (2007) 246803.

[18]   J. Chen, C. Jang, S. Xiao, M. Ishigami, M.S. Fuhrer, Intrinsic and extrinsic performance limits of graphene devices on SiO2, Nat Nano. 3 (2008) 206-209.

[19]   J. Chen, C. Jang, M. Ishigami, S. Xiao, W. Cullen, E. Williams, et al., Diffusive charge transport in graphene on SiO2, Solid State Communications. 149 (2009) 1080-1086.

[20]   F. Wang, Y. Zhang, C. Tian, C. Girit, A. Zettl, M. Crommie, et al., Gate-Variable Optical Transitions in Graphene, Science. 320 (2008) 206-209.

[21]   Z. Liu, K. Suenaga, P.J.F. Harris, S. Iijima, Open and Closed Edges of Graphene Layers,

Phys. Rev. Lett. 102 (2009) 015501.

[22] X. Jia, M. Hofmann, V. Meunier, B.G. Sumpter, J. Campos-Delgado, J.M. Romo-Herrera, et al., Controlled Formation of Sharp Zigzag and Armchair Edges in Graphitic Nanoribbons, Science. 323 (2009) 1701-1705.

[23] C.O. Girit, J.C. Meyer, R. Erni, M.D. Rossell, C. Kisielowski, L. Yang, et al., Graphene at the Edge: Stability and Dynamics, Science. 323 (2009) 1705-1708.

[24] G.M. Rutter, J.N. Crain, N.P. Guisinger, T. Li, P.N. First, J.A. Stroscio, Scattering and Interference in Epitaxial Graphene, Science. 317 (2007) 219-222.

[25] Y. Zhang, V.W. Brar, F. Wang, C. Girit, Y. Yayon, M. Panlasigui, et al., Giant phonon-induced conductance in scanning tunnelling spectroscopy of gate-tunable graphene, Nat Phys. 4 (2008) 627-630.

[26] E.J. Heller, K.E. Aidala, B.J. LeRoy, A.C. Bleszynski, A. Kalben, R.M. Westervelt, et al., Thermal Averages in a Quantum Point Contact with a Single Coherent Wave Packet, Nano Letters. 5 (2005) 1285-1292.

[27] G. Metalidis, P. Bruno, Green's function technique for studying electron flow in two-dimensional mesoscopic samples, Phys. Rev. B. 72 (2005) 235304.

[28] A. Freyn, I. Kleftogiannis, J. Pichard, Scanning Gate Microscopy of a Nanostructure Where Electrons Interact, Phys. Rev. Lett. 100 (2008) 226802.

[29] M.G. Pala, B. Hackens, F. Martins, H. Sellier, V. Bayot, S. Huant, et al., Local density of states in mesoscopic samples from scanning gate microscopy, Phys. Rev. B. 77 (2008) 125310.

[30] J.W.P. Hsu, N.G. Weimann, M.J. Manfra, K.W. West, D.V. Lang, F.F. Schrey, et al., Effect of dislocations on local transconductance in AlGaN/GaN heterostructures as imaged by scanning gate microscopy, Appl. Phys. Lett. 83 (2003) 4559.

[31] B. Hackens, F. Martins, T. Ouisse, H. Sellier, S. Bollaert, X. Wallart, et al., Imaging and controlling electron transport inside a quantum ring, Nat Phys. 2 (2006) 826-830.

[32] M.A. Topinka, B.J. LeRoy, R.M. Westervelt, S.E.J. Shaw, R. Fleischmann, E.J. Heller, et al., Coherent branched flow in a two-dimensional electron gas, Nature. 410 (2001) 183-186.

[33] K.E. Aidala, R.E. Parrott, E.J. Heller, R.M. Westervelt, Imaging electrons in a magnetic field, Cond-Mat/0603035. (2006).

[34] M.P. Jura, M.A. Topinka, L. Urban, A. Yazdani, H. Shtrikman, L.N. Pfeiffer, et al., Unexpected features of branched flow through high-mobility two-dimensional electron gases, Nat Phys. 3 (2007) 841-845.

[35] N. Shon, T. Ando, Quantum Transport in Two-Dimensional Graphite System, J. Phys. Soc. Jpn. 67 (1998) 2421-2429.

[36] M. Ishigami, J.H. Chen, W.G. Cullen, M.S. Fuhrer, E.D. Williams, Atomic Structure of Graphene on SiO2, Nano Letters. 7 (2007) 1643-1648.

[37] M. Katsnelson, A. Geim, Electron scattering on microscopic corrugations in graphene, Philosophical Transactions of the Royal Society A: Mathematical, Physical and Engineering Sciences. 366 (2008) 195-204.

[38] J. Chen, C. Jang, S. Adam, M.S. Fuhrer, E.D. Williams, M. Ishigami, Charged-impurity scattering in graphene, Nat Phys. 4 (2008) 377-381.

[39] L.A. Ponomarenko, R. Yang, T.M. Mohiuddin, M.I. Katsnelson, K.S. Novoselov, S.V. Morozov, et al., Effect of a High- kappa Environment on Charge Carrier Mobility in Graphene, Phys. Rev. Lett. 102 (2009) 206603.

[40] J. Yan, Y. Zhang, P. Kim, A. Pinczuk, Electric Field Effect Tuning of Electron-Phonon Coupling in Graphene, Phys. Rev. Lett. 98 (2007) 166802.

[41] C. Jang, S. Adam, J. Chen, E.D. Williams, S. Das Sarma, M.S. Fuhrer, Tuning the

Effective Fine Structure Constant in Graphene: Opposing Effects of Dielectric Screening on Short- and Long-Range Potential Scattering, Phys. Rev. Lett. 101 (2008) 146805.

[42] J. Martin, N. Akerman, G. Ulbricht, T. Lohmann, J.H. Smet, K. von Klitzing, et al., Observation of electron-hole puddles in graphene using a scanning single-electron transistor, Nat Phys. 4 (2008) 144-148.

[43] E. Rossi, S. Adam, S. Das Sarma, Effective medium theory for disordered two-dimensional graphene, Phys. Rev. B. 79 (2009) 245423.

[44] Y. Zhang, V.W. Brar, C. Girit, A. Zettl, M.F. Crommie, Origin of spatial charge inhomogeneity in graphene, Nat Phys. 5 (2009) 722-726.

[45] C. Chen, W. Bao, J. Theiss, C. Dames, C.N. Lau, S.B. Cronin, Raman Spectroscopy of Ripple Formation in Suspended Graphene, Nano Letters. 9 (2009) 4172-4176.

[46] S.V. Morozov, K.S. Novoselov, M.I. Katsnelson, F. Schedin, L.A. Ponomarenko, D. Jiang, et al., Strong Suppression of Weak Localization in Graphene, Phys. Rev. Lett. 97 (2006) 016801.

[47] J. Lee, J. Chae, C.K. Kim, H. Kim, S. Oh, Y. Kuk, Versatile low-temperature atomic force microscope with in situ piezomotor controls, charge-coupled device vision, and tip-gated transport measurement capability, Rev. Sci. Instrum. 76 (2005) 093701.

[48] S.H. Pan, E.W. Hudson, J.C. Davis, [sup 3]He refrigerator based very low temperature scanning tunneling microscope, Rev. Sci. Instrum. 70 (1999) 1459.

[49] T. Lohmann, K. von Klitzing, J.H. Smet, Four-Terminal Magneto-Transport in Graphene p-n Junctions Created by Spatially Selective Doping, Nano Letters. 9 (2009) 1973-1979.

[50] H. Yang, A.J. Mayne, M. Boucherit, G. Comtet, G. Dujardin, Y. Kuk, Quantum Interference Channeling at Graphene Edges, Nano Letters. 10 (2010) 943-947.

[51] X. Blasco, D. Hill, M. Porti, M. Nafria, X. Aymerich, Topographic characterization of AFM-grown SiO_{2} on Si, Nanotechnology. 12 (2001) 110.

[52] J. Chae, S.Y. Jung, S.J. Woo, H. J. Yang, H. Baek, J. Ha1, Y. J. Song, Y.-W. Son, N. B. Zhitenev, J. A. Stroscio, and Y. Kuk, to be published (2010)

[53] P.G. Silvestrov, K.B. Efetov, Charge accumulation at the boundaries of a graphene strip induced by a gate voltage: Electrostatic approach, Phys. Rev. B. 77 (2008) 155436.

FIGURE CAPTIONS

Fig. 1: (A) Schematic diagram of AFM operated at cryogenic temperature. This unit is kept inside a UHV tube that is inserted in a helium Dewar. A laser reflection from the back of a cantilever is detected by a quadrant photodiode. Piezoelectric motors are mounted to align the detection mechanism and the sample coarse movements. (B) CCD images of a GD with a long-range optical microscope installed inside UHV AFM chamber. C) Operational principle of SGM. As an AFM cantilever scans a line, the controlling computer remembers the topography. After the scan a tip bias is applied to the tip and follows the topography, such that the tip follows the same distance away from the sample.

Fig. 2: (A) An optical microscope image of a fabricated GD. A faint dark object is a single-layer graphene and bright parts are contact electrodes. (B) A typical graphene resistance versus back gate bias voltage after loading into AFM and several annealing process. Red data was taken as increasing the bias and the green curve was obtained as ramping down. (C)-(D) Macroscopic transport measurement data before inserting into AFM chamber (C) and after annealing at 380K for 6 hours (D).

Fig. 3: (A) STM topography of a monolayer graphene on a Si-terminated SiC. (B) STS data on the surface of the monolayer graphene.

Fig. 4: (A) AFM topography of a GD measured in contact mode. (B) An AFM topography in non-contact mode. Maximum vertical corrugation is ~ 2nm.

Fig. 5: (A) An AFM topography of 800 x 800 nm area on a GD. (B)-(L) SGM data on the same area at tip gating bias of −2.5 V, −2.0 V, −1.5 V, −1.0 V, −0.5 V, 0 V, 0.5 V, 1.0 V, 1.5 V, 2.0 V and 2.5 V respectively. (M) Color-coded scale bar of conductance change for SGM data

Fig 6: (A) An AFM topography of geometrical defect. (B)-(F) Corresponding SGM signals with tip gating bias of −2 V, −4 V, 0 V, 2 V and 4V respectively. (G) Color-coded scale bar of conductance change for SGM data

Fig. 7: SGM micrograph of a GD in which the Dirac point is -20 V of the back gate voltage with tip gate bias of −1 V (A) and −2 V (B). Strong conductance enhancement at the edge was observed with −2 V of tip bias which is more close to Dirac point.

Fig. 1:   Chae et al

(A)

V_{tip}
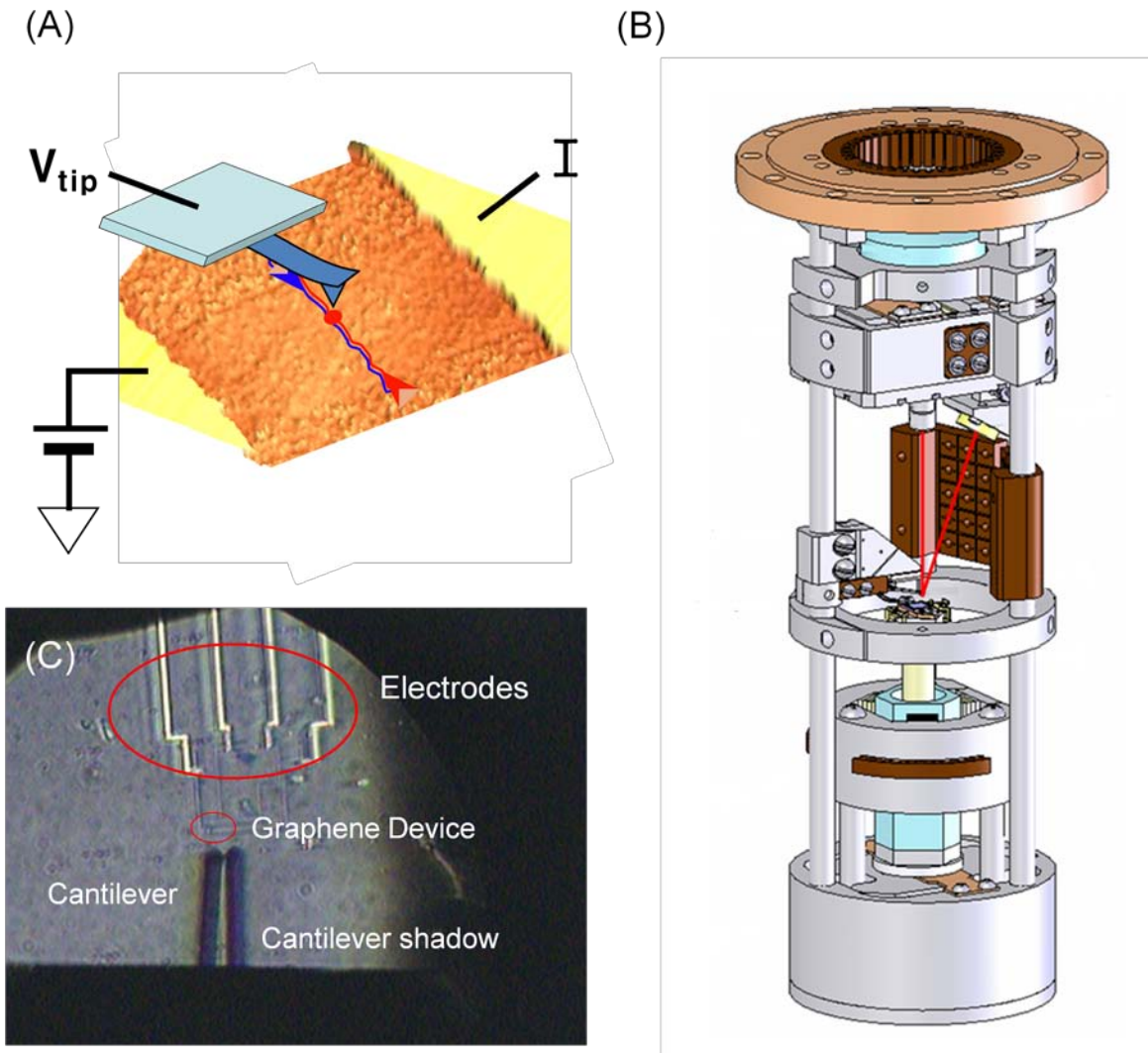
(B)

(C)

Electrodes

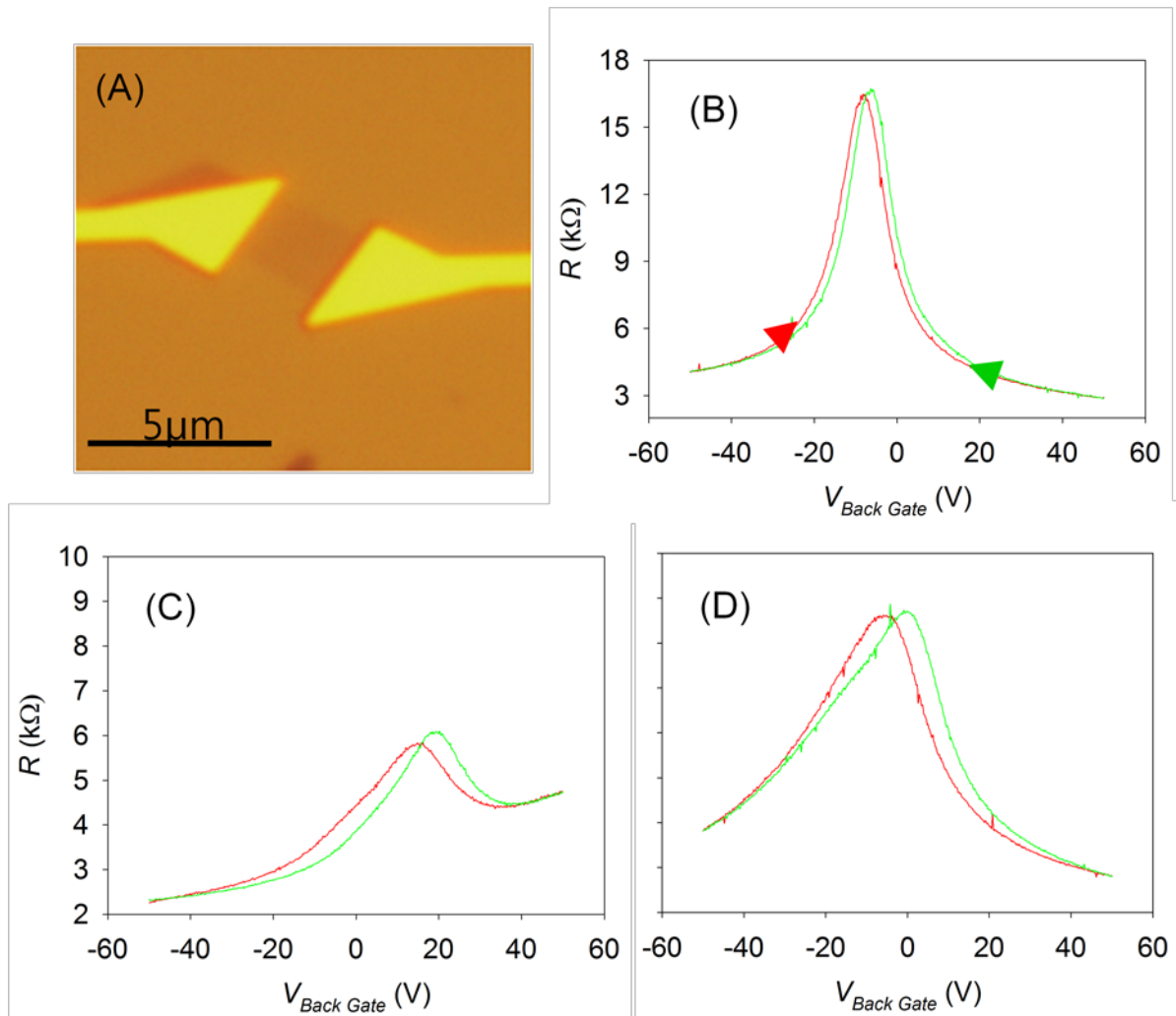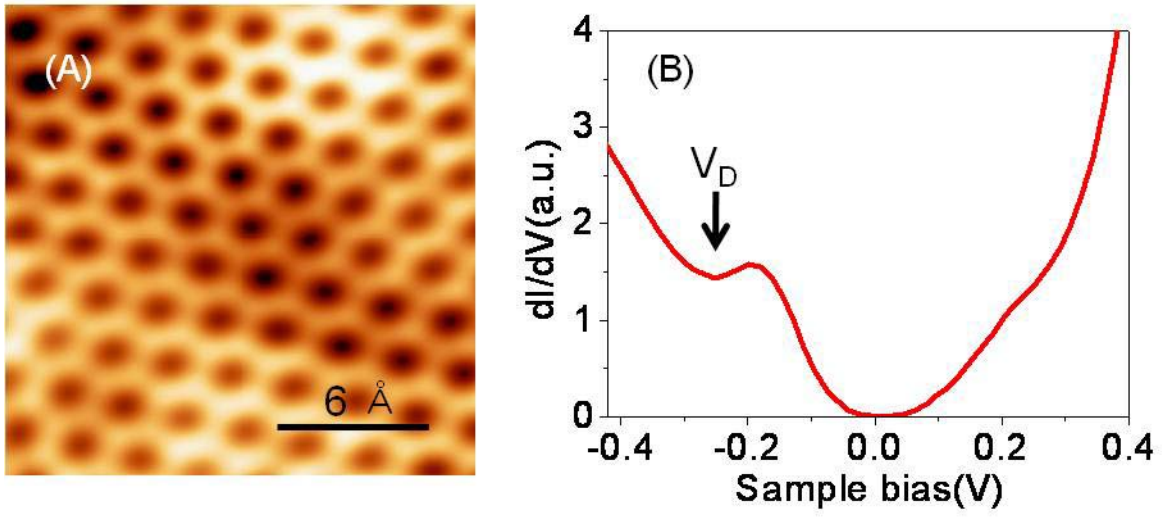Graphene Device

Cantilever

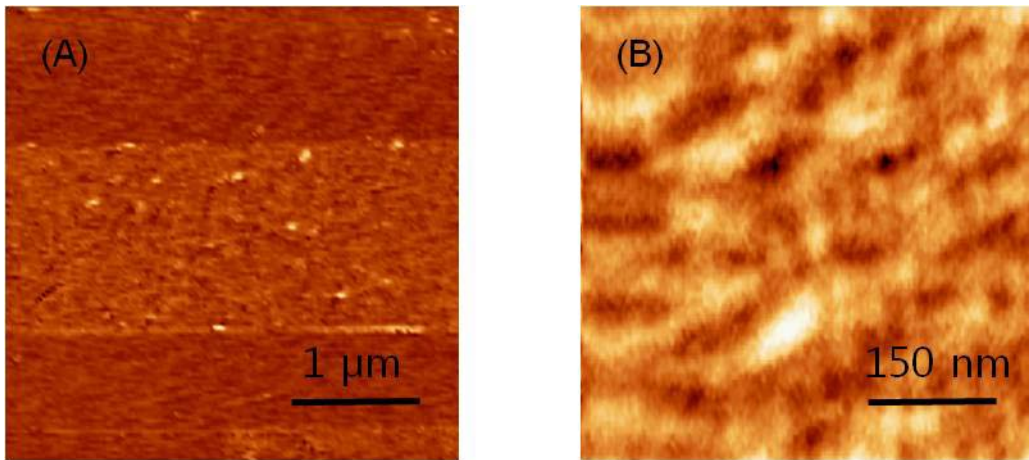Cantilever shadow

Fig. 2:   Chae et al

Fig. 3: Chae et al.

Fig. 4: Chae et al

Fig. 5: Chae et al

(A) 300 nm

(B) $V_{tip} = -2.5$ V

(C) -2.0 V

(D) -1.5 V

(E) -1.0 V

(F) -0.5 V

(G) 0 V

(H) 0.5 V

(I) 1.0 V
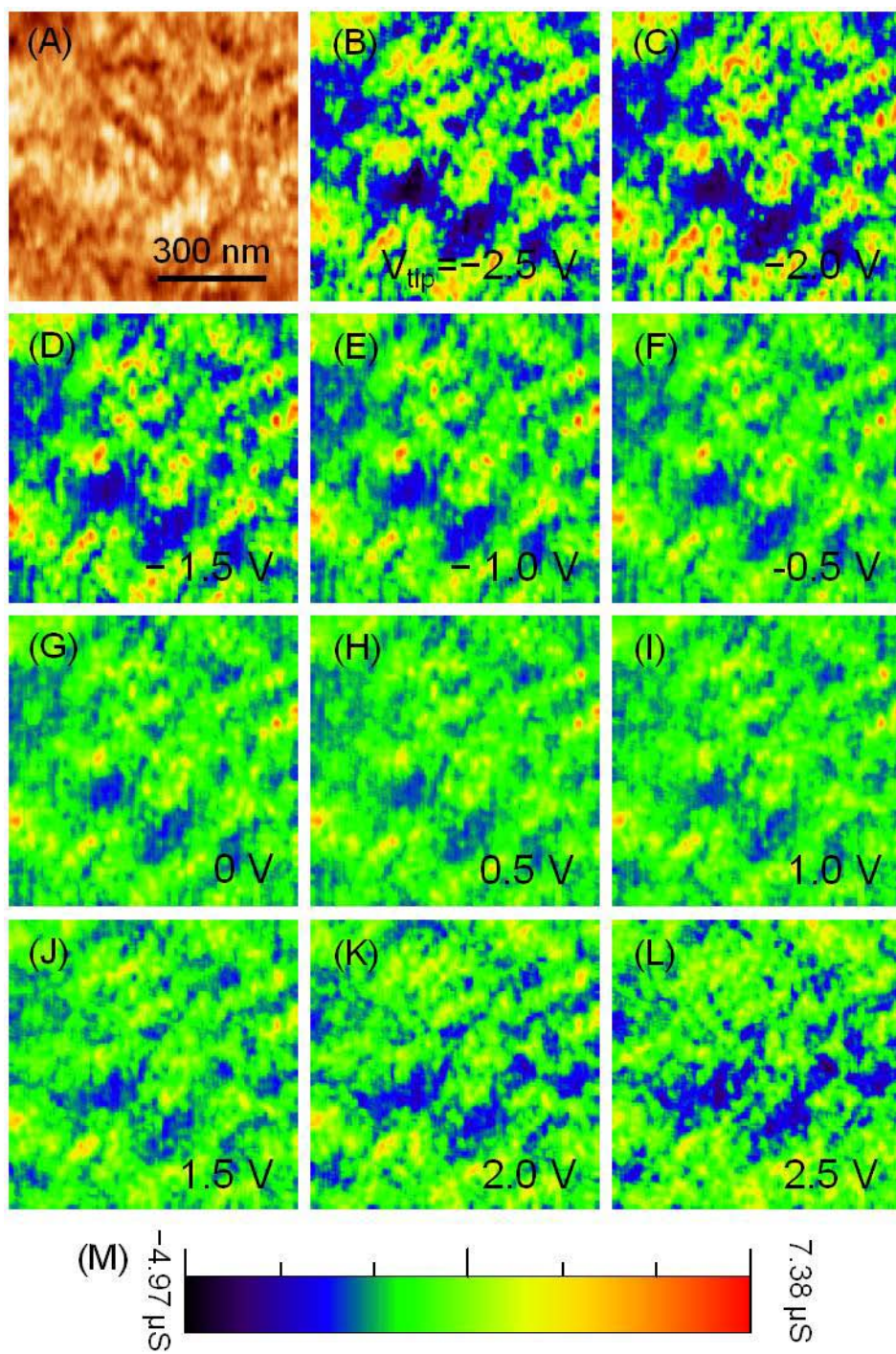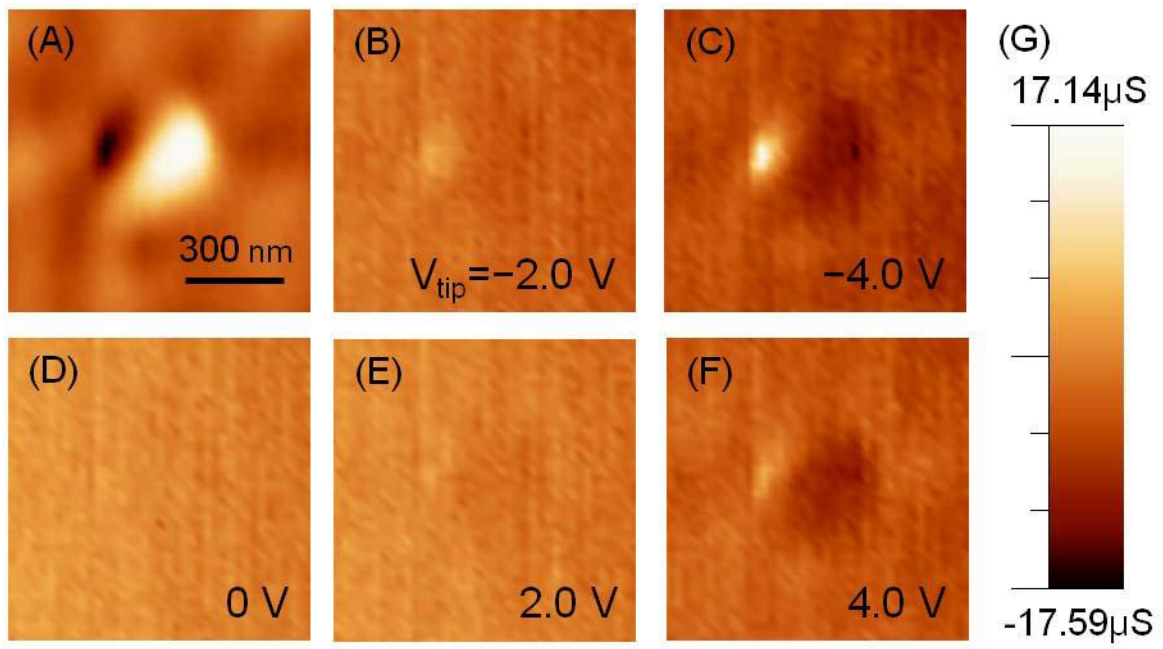
(J) 1.5 V

(K) 2.0 V

(L) 2.5 V

(M) -4.97 µS   7.38 µS

Fig. 6: Chae et al

Fig. 7: Chae et al

(A)

-68 nS

120 nS

(B)

-72 nS

524 nS